Life Sciences 329 (2023) 121945

Contents lists available at ScienceDirect

Life Sciences

journal homepage: www.elsevier.com/locate/lifescie

Exosomal miR-21 determines lung-to-brain metastasis specificity through the DGKB/ERK axis within the tumor microenvironment

Tung-Yu Tiong [a,b], Mei-lin Chan [c,d], Chun-Hua Wang [e,f], Vijesh Kumar Yadav [g], Narpati Wesa Pikatan [h], Iat-Hang Fong [g], Chi-Tai Yeh [g,i], Kuang-Tai Kuo [a,b], Wen-Chien Huang [c,d,*]

[a] Division of Thoracic Surgery, Department of Surgery, School of Medicine, College of Medicine, Taipei Medical University, Taipei 110, Taiwan
[b] Division of Thoracic Surgery, Department of Surgery, Taipei Medical University—Shuang Ho Hospital, New Taipei City 235, Taiwan
[c] Division of Thoracic Surgery, Department of Surgery, MacKay Memorial Hospital, Taipei 104, Taiwan
[d] Department of Medicine, MacKay Medical College, New Taipei City 252, Taiwan
[e] Department of Dermatology, Taipei Tzu Chi Hospital, Buddhist Tzu Chi Medical Foundation, New Taipei City 231, Taiwan
[f] School of Medicine, Buddhist Tzu Chi University, Hualien 970, Taiwan
[g] Department of Medical Research & Education, Taipei Medical University—Shuang Ho Hospital, New Taipei City 235, Taiwan
[h] Graduate Program, Faculty of Medicine, Universitas Gadjah Mada, Yogyakarta 55281, Indonesia
[i] Continuing Education Program of Food Biotechnology Applications, College of Science and Engineering, National Taitung University, Taitung 95092, Taiwan

ARTICLE INFO

Keywords:
Lung cancer
Brain metastasis
Cancer stem cell niche
Extracellular vesicles (EVs)
DGKB/ERK/STAT3 signaling
OncomiR miR-21
ERK inhibitor

ABSTRACT

Background: Brain metastasis affects 20–40 % of lung cancer patients, severely diminishing their quality of life. This research focuses on miR-21, overexpressed in these patients and inversely associated with DGKB in the ERK/STAT3 pathway, suggesting a dysregulated pathway with therapeutic potential.
Aims: The objective was to investigate miR-21's role in lung cancer patients with brain metastases and whether targeting this pathway could improve treatment outcomes. We also examined the miR-21 content in tumor spheres-derived extracellular vesicles (EVs) and their influence on ERK/STAT3 signaling and metastasis.
Materials and methods: Tumor spheres were created from metastatic lung cancer cells. We studied miR-21 levels in these spheres, their impact on macrophage polarization, and the transition of nonmetastatic lung cancer cells. Furthermore, we analyzed miR-21 content in EVs derived from these spheres and their effect on ERK/STAT3 signaling and metastasis potential.
Key findings: We found tumor spheres had high miR-21 levels, promoting macrophage polarization and, epithelial–mesenchymal transition. These spheres-derived EVs, enriched with miR-21, accelerated ERK/STAT3 signaling and metastasis. Silencing miR-21 and inhibiting ERK signaling with ulixertinib notably mitigated these effects. Moreover, ulixertinib reduced brain metastasis incidence and increased survival in a mouse model and led to reduced tumor sphere generation and miR-21 levels in EVs.
Significance: Our study highlights the exacerbation of lung-to-brain metastasis *via* miR-21-rich EV secretion. This underlines the therapeutic promise of targeting the miR-21/ERK/STAT3 pathway with ulixertinib for managing brain metastasis from lung cancer.

1. Introduction

Lung cancer remains one of the first causes of neoplastic-associated mortality despite advances in therapeutics [1]. Non–small-cell lung cancer (NSCLC) accounts for approximately 85 % of all lung cancer cases [2]. The prognosis of metastatic NSCLC is poor, with an estimated 5-year relative survival rate is approximately 6–8 % [3,4]. A major distant metastatic site in NSCLC is the brain, and this disease is often associated with acquired chemoresistance and recurrence, all of which contribute to the poor survival rates of patients [5]. Thus, the crucial task is to identify the mechanisms through which NSCLC cells metastasize to the brain and translate this knowledge to develop new interventions.

Accumulating evidence suggests that intracellular communications between cancer cells and stromal cells within the tumor

* Corresponding author at: Department of Medicine, MacKay Medical College, New Taipei City 252, Taiwan.
E-mail address: t102@mmc.edu.tw (W.-C. Huang).

https://doi.org/10.1016/j.lfs.2023.121945
Received 1 April 2023; Received in revised form 7 July 2023; Accepted 13 July 2023
Available online 16 July 2023

microenvironment (TME) should also be considered when therapeutics are designed. One emerging messenger within the TME is extracellular vesicles (EVs); they contain various cytokines, signaling molecules, nucleic acids (coding or noncoding RNAs and DNA), and proteins, and they serve as an intracellular communication tool [6]. A recent seminal study demonstrated that EVs from different cancer types play a prominent role in determining the site of distant metastasis [7]. Another study indicated that EVs released by lung cancer cells contributed to increased levels of proinflammatory marker S100A16 and the incidence of brain metastasis [8]. A related report indicated that hypoxic lung cancer cells secreted exosomes containing miR-23a into the TME and inhibited tight junction protein ZO-1 expression, resulting in increased vascular permeability and promoting cancer trans-endothelial migration [9]. This suggests that inhibiting cancer-associated EVs may provide important insight into impeding distant metastasis.

In lung cancer, EVs have been shown to carry miRNAs that can influence recipient cells and their surrounding environment, promoting tumorigenesis, angiogenesis, immune escape, and metastasis [10]. A notable miRNA in this context is miR-21, which is often overexpressed in lung cancer cells and carried by EVs[11]. Diacylglycerol Kinase Beta (DGKB), an enzyme that plays a role in signal transduction pathways, including the ERK/STAT3 pathway[12]. The ERK/STAT3 signaling pathway is crucial for many cellular processes, including cell growth, proliferation, differentiation, and apoptosis, and its dysregulation is a common feature in many cancers, including non-small cell lung cancer (NSCLC)[13,14]. Understanding this EV/miRNA/DGKB/ERK/STAT3 axis in lung cancer can provide important insights into the mechanisms of lung cancer progression and might offer potential targets for therapeutic intervention. For instance, strategies aimed at blocking the release of EVs, inhibiting miR-21, or restoring DGKB function might help to inhibit the ERK/STAT3 pathway and thereby limit the progression of lung cancer. Nevertheless, more research is needed to fully explore these possibilities and their potential applications in the treatment of lung cancer.

Our study, based on an extensive literature review, identified elevated levels of oncomiR miR-21 in lung adenocarcinoma and squamous carcinoma, with an inverse correlation to its target gene, diacylglycerol kinase beta (DGKB). Brain-metastatic lung cancer cell-derived EVs (BMets_1) enriched with miR-21 promoted metastasis and self-renewal in nonmetastatic primary lung cancer cells (P1), and induced macrophage M2 polarization. miR-21 silencing reduced metastasis and self-renewal, aligning with decreased miR-21 in cancer EVs. The Erk inhibitor ulixertinib effectively suppressed lung cancer metastasis, reducing cell migration, invasion, and self-renewal, linked to miR-21 and Erk/STAT3 downregulation, and DGKB upregulation. Ulixertinib alone or with miR-21 silencing greatly suppressed lung tumorigenesis and brain metastasis in patient-derived xenograft models, highlighting the therapeutic potential of the miR-21/DGKB/ERK axis in metastatic NSCLC. Further research will expand on these interactions and ulixertinib's clinical potential.

2. Materials and methods

2.1. Ethics approval and consent to participate

Clinical samples were collected at MacKay Memorial Hospital (Taipei, Taiwan). All enrolled patients provided written informed consent for their tissues to be used for scientific research. The study was approved by the Institutional Review Board (IRB) of MacKay Memorial Hospital (IRB 20MMHIS500e), was conducted following the recommendations of the Declaration of Helsinki for biomedical research (MacKay Memorial Hospital Taipei, Taiwan), and followed the standard institutional protocol for human research. The animal study protocol was approved by the Animal Care and User Committee at MacKay Memorial Hospital (Affidavit of Approval of Animal Use Protocol # MacKay Memorial Hospital-MMH-A-S-111-10).

2.2. Cell culture, clinical sample and primary cells characteristics

Human lung cancer cell lines H1623 and H2085 were purchased from the American Type Culture Collection (USA) and cultured and maintained under conditions recommended by the supplier. Clinical samples from patients diagnosed with either nonmetastatic or brain-metastatic lung cancer were collected at MacKay Memorial Hospital (IRB 20MMHIS500e) between 2015 and 2018 and stored in liquid nitrogen for long-term storage and use. P1 cells were collected from one of the patients from this cohort (non–small-cell lung cancer; primary tumor without lymph node and brain metastases), and BMets_1 cell was surgically collected from a patient with brain metastasis. All patients provided written informed consent before they participated in the study. The clinical parameters of the deidentified clinical samples are listed in Table 1. Additionally, to characterize the primary cells originating from epithelial tissue, we performed a morphological analysis using an inverted optical microscope. The images showed that the primary cells both P1 and BMets_1, which were polygonal or fusiform in shape, clustered together, exhibiting complete loss of contact inhibition. Moreover, immunofluorescence imaging revealed co-expression of stromal cell marker vimentin (red), epithelium cell marker CK7 (green) and nuclear stain DAPI (Blue) to demonstrate its purity. *in vitro*, which was also detected in the nucleus (Supplementary Fig. S1).

2.3. Sequencing data collection and analysis

The GEO database was used to collect the patient's lung cancer data (https://www.ncbi.nlm.nih.gov/geo/), the GEO datasets GSE14814 and GSE68465 were applied to explore the expression of DGKB expression and its clinical correlation with lung cancer and associated genes. Through the R software package, the download files were handled.

2.4. Cell viability test

Cell viability was determined using the Cell Counter Kit-8 (CCK-8; Dojindo, Kumamoto, Japan). Cells were seeded (5.0×10^3 cells/well) in 96-well plates. The cells were then treated with ulixertinib (BVD-523, VRT752271, SelleckChem, USA) at various concentrations ranging from 0 to 25 μM for 48 h before CCK-8 reagent was added. The optical diffraction values were determined at 450 nm, with the viability of the samples expressed in percentages.

2.5. Quantitative real-time PCR (qPCR) analysis

The isolation of total RNA from cells was carried out using the TRIzol reagent by Invitrogen. To measure miRNA levels, we converted the RNA into cDNA using miRNA-specific reverse transcriptase primers, which

Table 1
Clinicopathological features of NSCLC patients (N = 20).

Parameters	N	%
Age (years)	58.4 ± 9.8	
Gender (male)	20	100 %
Smoke (n/%)	15	75 %
Histology		
Adenocarcinoma (n/%)	12	60 %
Squamous cell carcinoma (n/%)	8	40 %
Pathological grade		
Poorly differentiated (n/%)	17	75 %
Moderately differentiated (n/%)	3	25 %
Well-differentiated (n/%)	0	0 %
Tumor size		
>5 cm (n/%)	8	40 %
≤5 cm (n/%)	12	60 %
Brain metastasis		
Positive (n/%)	10	50 %
Negative (n/%)	10	50 %

were part of the TaqMan MicroRNA Reverse Transcription kit from Applied Biosystems, Life Technologies Corp., California, USA. For the quantitation of mRNA, the RNA was transcribed into cDNA utilizing the PrimeScript RT reagent kit produced by Takara, located in Dalian, China. We then performed quantitative RT-PCR on the cDNA using an ABI 7500 instrument from Applied Biosystems. The mRNA levels were determined using FastStart Universal SYBR Green Master (Rox) supplied by Roche, USA. Meanwhile, the TaqMan® MicroRNA Assay kit by Applied Biosystems was used for miRNA measurement. Finally, we calculated the relative expression of miRNA and mRNA using the inverse log of the ΔΔCT method, normalizing the results to U6 and GAPDH.

The primer sequences used are presented in Table 2.

2.6. Macrophage polarization

Monocytic cell line THP-1 cells were treated with 100 nM phorbol-12-myristate-13-acetate for 24 h, and the adherent THP-1 cells (M0 macrophages) were subsequently cocultured with NSCLC cells and seeded in the upper chamber of Transwell inserts (pore size: 0.4 μm, Corning, USA) for an additional 48 h. For ulixertinib treatment, both H1623 and H2085 cells were treated with ulixertinib (1 μM, 24 h) before coculturing with THP-1(M0 macrophages). M1–M2 polarization was then determined using qPCR. M2 cytokines were detected using enzyme-linked immunosorbent assay kits (IL-6, Cat No. BMS213HS, ThermoFisher Scientific, USA; LEGEND MAX Total TGF-β1 ELISA Kit). The reactions were conducted per the instructions provided by the vendors.

2.7. Overexpression and knockdown experiments

The expression of miR-21-5p was either suppressed using the miR-21-5p inhibitor (Catalog No. HLTUD0371; Mission®; sequence: 5′-CUUCAACAUCAGUCUGAUAAGCUA-3′) or enhanced using the miR-21-5p mimic (Catalog No. HMI0371; Mission®) with a sense strand (5′-UAGCUUAUCAGACUGAUGUUGAA-3′) and an antisense strand (5′-UCAACAUCAGUCUGAUAAGCUAUU-3′). A negative control (NC) was also employed, featuring a sense strand (5′-UUCUCCGAACGUGUCACGUTT-3′) and an antisense strand (5′-ACGUGACACGUUCGGAGAATT-3′). The transfection was conducted following the manufacturer's instructions. Moreover, lentiviral vectors carrying the hsa-miR-21-5p-inhibitor (miR-21-5p si), along with a control vector, were developed by GeneChem Co., Ltd. For *in vitro* transfection, BMets_1 (1.0×10^5 cells/ml) were infected with miR-21-5p si, combined with Lipofectamine® 2000 (Invitrogen Thermo Fisher Scientific, Inc.). Post 8–12 h of infection, the lentivirus-laden culture media was removed after centrifugation at 300 ×*g* for 5 min at ambient temperature. The cells were then incubated in their respective complete culture media for a further 48–72 h. Following this, the cells were sorted with 2 μg/ml puromycin to create stable cell lines for subsequent experiments. The entire lentivirus infection and construction process was carried out in strict adherence to the practice guidelines at the certified BSL-2 laboratory in the MacKay Memorial Hospital, Taiwan.

2.8. Sphere formation assay

The self-renewal capacity of the NSCLC cells subjected to various treatments was examined *via* a sphere formation assay, which was carried out based on a method outlined previously [15]. In summary, each well was seeded with 1×10^3 cells that were either untreated or had undergone treatment. The cells were cultured in a 1 mL serum-free DMEM medium, enhanced with 20 ng/mL B27 (Invitrogen, ThermoFisher Scientific Inc.) and 10 ng/mL epidermal growth factor (BD Biosciences). This was all set in 12-well ultra-low attachment plates and incubated at 37 °C in a humidified atmosphere containing 5 % CO_2. Non-adherent spheroids with diameters exceeding 90 μm were identified and tallied, with their dimensions subsequently measured using an ocular micrometer.

2.9. Extracellular Vesicles Isolation and Conditioned Medium Treatment

The extracellular vesicles (EVs) from both clinical non-small cell lung cancer (NSCLC) samples and cell lines (BMet_1 and CSCs) using a protocol previously published [16]. This process involved collecting the serum-free culture medium and sequentially centrifuging it at different speeds - initially at 300 ×*g* for 10 min, then 2000 ×*g* for 20 min, followed by 10,000 ×*g* for 30 min. The resulting pellets were discarded while the supernatant underwent another round of centrifugation at 110,000 ×*g* for 80 min at 4 °C to accumulate the EVs. These pelleted EVs were then diluted in phosphate-buffered saline (PBS) and centrifuged again at 110,000 ×*g* for 80 min at 4 °C. The resulting EVs were re-suspended in PBS for further analysis. To verify the successful collection of EVs and their relative quantities, we conducted Western blots using the EV-specific markers CD63 and CD9. Simultaneously, we generated conditioned media (CM) by culturing cells in the standard medium at a density of 200,000 cells per flask. After 24 h, the cells were washed and further incubated in RPMI medium devoid of FBS for an additional 48 h. To remove any remaining cells and cell debris, the collected media was centrifuged for 10 min at 10,000 ×*g* and 4 °C. The resulting supernatants were then utilized for our conditioned media studies. Non-small cell lung cancer (NSCLC, P1) cells were cultivated at a density of 75,000 cells per well in six-well plates. After 48 h of growth in the standard medium, these cells were then incubated for an additional 96 h, either in the conditioned media or with extracellular vesicles (EVs).

2.10. SDS-PAGE and Western blots

Total proteins were extracted from both the NSCLC cells and exosomes using RIPA buffer (Millipore), which was augmented with a protease and phosphatase inhibitor cocktail (1:100 ratio) and PMSF (Beyotime). These protein lysates were then quantified with the aid of a BCA Protein Assay Kit (Thermo Fisher Scientific). Following this, protein samples were separated using 10 % SDS-PAGE and then transferred onto nitrocellulose membranes (0.45 μm, Millipore). Afterward, the membranes were blocked in TBST containing 5 % nonfat milk. They were

Table 2
The sequences of primers used in qRT-PCR.

Gene symbol	Forward	Reverse
DGKB	CCTATCAGGCGGTCTGAGAAT	GGAACACGTATTTGCAGGAGAAG
ERK	ATGTCATCGGCATCCGAGAC	GGATCTGGTAGAGGAAGTAGCA
STAT3	CAGCAGCTTGACACACGGTA	AAACACCAAAGTGGCATGTGA
INF-γ	AGCGATTCCAGTATCCTCACT	CCAGGCTAAGCACTAGAAAGAGT
TNF-α	CCTCTCTCTAATCAGCCCTCTG	GAGGACCTGGGAGTAGATGAG
CD206	TCCGGGTGCTGTTCTCCTA	CCAGTCTGTTTTTGATGGCACT
CD163	GCGGGAGAGTGGAAGTGAAAG	GTTACAAATCACAGAGACCGCT
GAPDH	ATCAAGAAGGTGGTGAAGCAGG	GTCATACCAGGAAATGAGC
hsa-miR-21-5p-RT	CTCAACTGGTGTCGTGGAGTCGGCAATTCAGTTGAGTCAACA	
hsa-miR-21-5p	ACACTCCAGCTGGGTAGCTTATCAGACTGA	TGGTGTCGTGGAGTCG
hsa-U6-RT	GTCGTATCCAGTGCAGGGTCCGAGGTATTCGCACTGGATACGACAAAATA	
U6	CTCGCTTCGGCAGCACA	AACGCTTCACGAATTTGCGT

then washed and left to incubate overnight in a cold environment with an array of primary antibodies, including CD63 and CD9 (1:500 ratio, Cell Signaling Technology), Slug (1:400 ratio, CST), E-cadherin (1:800 ratio, CST), vimentin (1:600 ratio, CST), phosphor-ERK (1:400 ratio, CST), phospho-STAT3 (1:500 ratio, CST), STAT3 (1:800 ratio, CST), survivin (1:600 ratio, Abcam), DGKB (1:500 ratio, CST), Erk1/2 (1:500 ratio, Abcam), PARP (1:500 ratio, Abcam), GAPDH, and β-actin (11,000 ratio, CST). Finally, the signals were detected using enhanced chemiluminescence (Thermo Fisher Scientific) and an electrochemiluminescence imaging system (Tanon, 5200).

2.11. In vivo evaluation of NSCLC inhibitory functions of ulixertinib

Non-obese diabetic/severe combined immunodeficiency (NOD/SCID) female mice (6 weeks old) were supplied by the animal care facility of MacKay Memorial Hospital. The animal study protocol was approved by the Animal Care and User Committee at MacKay Memorial Hospital (Affidavit of Approval of Animal Use Protocol # MacKay Memorial Hospital-MMH-A-S-111-10). For *in vivo* evaluation of ulixertinib, we established a patient-derived xenograft (PDX) mouse model by injecting the mice with BMets_1 cells (mixed with Matrigel, 6×10^6 cells per injection) intrathoracically. The mice were anaesthetized through the intraperitoneal (i.p) injection of xylazine and ketamine. Insulin syringes with 30-gauge hypodermic needles were used to inject BMets_1 cell into the thorax. After tumor injection, the mice were allowed to recover, and the tumorigenic process was monitored using bioluminescence (IVIS system, Caliper, USA). The tumor burden was semi-quantitatively measured based on the total photon flux over time. Mice were randomly divided into four groups: the vehicle control group (PBS i.p injection, 5 times/week), ulixertinib group (100 mg/kg, i.p, 5 times/week), miR-21-5p si group (injection with BMets_1 cells transfected with miR-21-5p inhibitor, described in the upper section), and combined group (mice with BMets_1 [miR-21-5p silenced] cells receiving ulixertinib treatment [100 mg/kg, i.p, 5 times/week]). After the experiments, mice were humanely sacrificed, and tumor samples were collected for further analyses.

2.12. Immunohistochemistry and immunofluorescence staining (IFS)

The lungs of the sacrificed mice were excised and fixed in formalin for 24 h, paraffin-embedded, and sectioned (5-μm thickness). Sections were then dewaxed in xylene, rehydrated through sequential ethanol incubation, and washed in deionized water. For staining, sections were first blocked in PBS with 1 % BSA, 1 % donkey serum, 0.3 % Triton X-100, and 0.01 % sodium azide for 1 h at room temperature. Primary antibodies were diluted in blocking buffer and incubated with the sections overnight in cold. Subsequently, sections were washed in PBST three times and incubated with secondary antibodies in a blocking buffer for 1 h at room temperature. Stained sections were then observed under a microscope and micrographs were produced. For the immunofluorescent staining of the cells, the slides were first blocked in PBS with 5 % Bovine Serum Albumin (BSA). They were then incubated overnight at 4 °C with primary antibodies Cytokeratin 7 antibody (CK7; 1 μg/ml, ab53123) and vimentin (2 μg/ml, ab92547). Post rinsing with PBS, they were further incubated for 30 min at 37 °C with the secondary antibody. DAPI was subsequently added for staining the nuclei. Images were captured using an Axio Vert A1 inverted fluorescence microscope.

2.13. Statistical analysis

All the experimental data are presented as means ± standard deviations and graphed using GraphPad Prism software (GraphPad Software, La Jolla, CA, USA). Student's *t*-test was used to analyze the differences between the groups. Comparisons among groups were analyzed using a one-way analysis of variance with Tukey's *post hoc* tests. $P < 0.05$ was considered statistically significant. All experiments were performed in triplicate.

3. Results

3.1. miR-21 elevation was pronounced in the patients with brain-metastasized lung cancer and associated with a poor survival rate

Through our literature review, we discovered that miRNA expression in brain metastases from cancer was prominent. Among these, miR-21 emerged as one of the most significantly upregulated microRNAs in samples from brain metastases [17–20]. Additionally, lung cancer patients exhibiting higher levels of miR-21 expression notably demonstrated a significantly diminished survival rate compared to those presenting lower miR-21 expression (Fig. 1A). We then applied online prediction algorithm and observed DGKB was a target of miR-21-5p (insert, Fig. 1B) in a collection of samples from patients with lung cancer (GSE14814); in these samples, suppressed DGKB expression was significantly associated with a higher risk of lung cancer (lower panel, Fig. 1B). In addition, we observed a strong negative correlation between miR-21-5p expression and DGKB in two cohorts consisting of patients with lung adenocarcinoma (n = 512) and lung squamous carcinoma (n = 475); in these groups, miR-21-5p expression was significantly elevated, whereas DGKB expression was markedly suppressed (GSE68465, Fig. 1C). We then analyzed our own clinical samples and noted a similar phenomenon; brain-metastatic samples exhibited significantly higher miR-21-5p expression but lower DGKB expression than did the nonmetastatic primary samples (Fig. 1D). Similarly, another study reported a positive correlation between miR-21 level and brain metastasis in a cohort of patients with non–small-cell lung cancer (total of 132 patients with NSCLC-68 with and 64 without brain metastasis) [21]. Further, the expression of DGKB and miR-21-5p was analyzed in MacKay Memorial Hospital-NSCLC tumor tissue corresponding to normal counterpart, confirming the above-observed expression (Fig. 1E).

3.2. miR-21-enriched EVs secreted by brain-metastatic lung cancer cells promoted metastatic potential in nonmetastatic cells

Studies have indicated that cancer cells transform the TME through the secretion of various signaling molecules such as EVs [22] and that oncomiR-enriched EVs play a key role in promoting lung tumorigenesis, with miR-21-containing EVs being an example [23]. In this study, we first observed that the conditioned medium (CM) and extracellular vesicles (EVs) from BMets_1 cell promoted epithelial–mesenchymal transition (EMT) and metastatic potential (Fig. 2A) of nonmetastatic primary lung cancer cells (P1). This increased EMT and metastatic ability was accompanied by an increased expression of slug and vimentin, whereas that of E-cadherin was decreased (Fig. 2B). In addition, CM-EVs treated P1 cells exhibited a stronger self-renewal ability, as reflected by the increased number of tumor spheres generated under serum-deprived conditions (Fig. 2C). Subsequently, EVs from the culture media of P1, BMets_1 cells, and cancer stem-like cells (CSCs; spheres generated from BMets_1 cells), as demonstrated by western blot analysis, showing the induced expression of the exosomal specific markers *i.e.* CD63 and CD9 (upper panel, Fig. 2D), and noted that miR-21-5p expression was markedly higher in EVs isolated from the BMets_1 and CSCs groups (Fig. 2D). When P1 cells were cultured only with EVs isolated from the BMets_1 cells and CSCs, both migratory (upper panels, Fig. 2E) and invasive (lower panels, Fig. 2E) abilities were significantly enhanced in comparison with their P1 counterparts. Notably, the EVs from both the BMets_1 cells and CSCs also increased the self-renewal ability of P1 cells, as reflected by the markedly increased number of tumor spheres generated (Fig. 2F); these observations were supported by Western blotting, where P1 cells incubated with EVs from BMets_1 cells and CSCs exhibited significantly increased expressions of slug and vimentin but decreased E-cadherin expression (Fig. 2G).

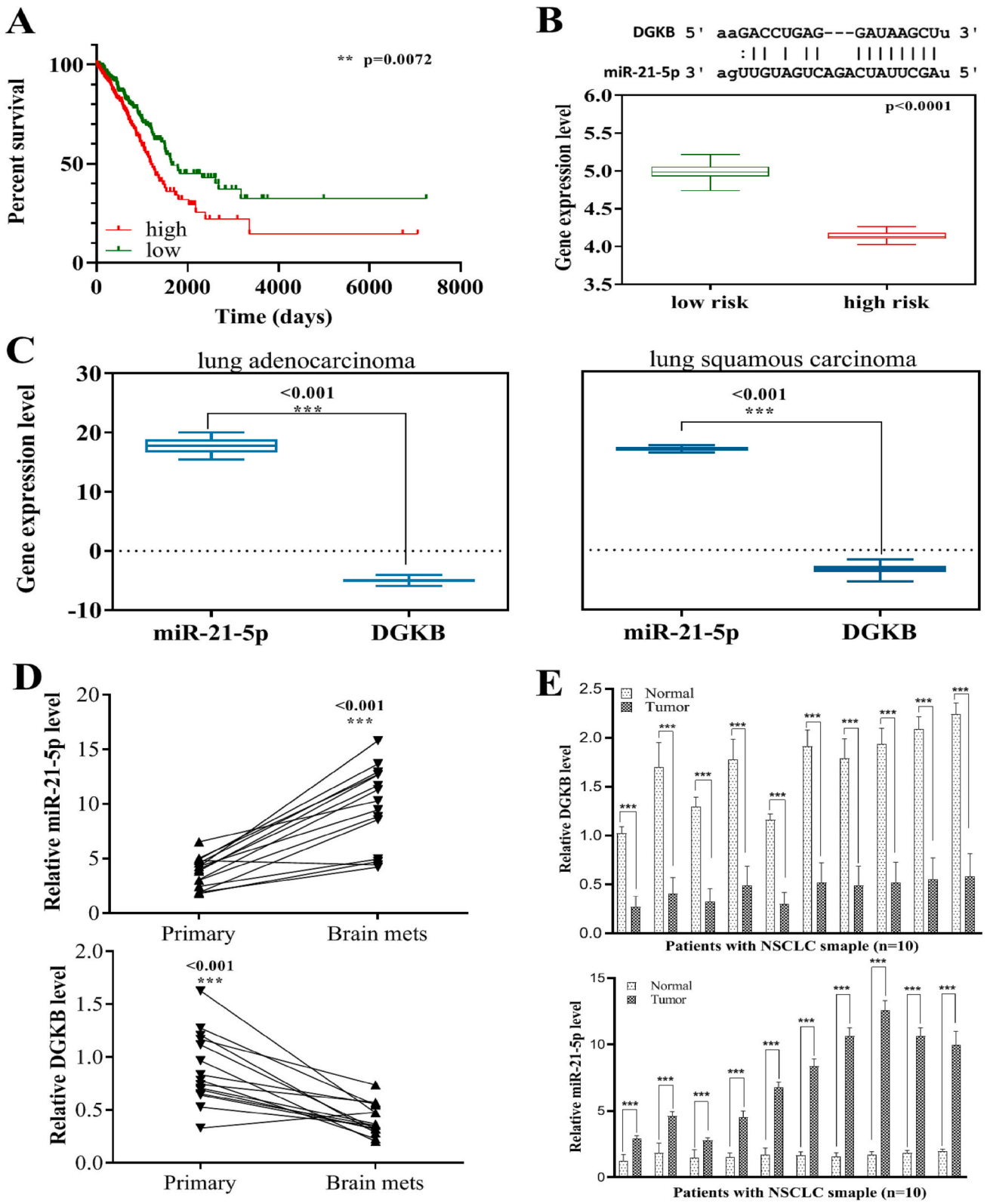

Fig. 1. Upregulation of miR-21-5p and downregulation of diacylglycerol kinase beta (DGKB) are associated with poor prognosis for patients with lung cancer. (A) Increased miR-21 expression levels in patients with lung cancer were associated with a shorter survival rate ($p = 0.0028$, $n = 504$, The Cancer Genome Atlas database). (B) In another cohort, patients with a high risk of developing lung cancer had significantly lower DGKB expression; the insert indicates that DGKB is a potential target of miR-21-5p. (C) In two lung cancer cohorts (adenocarcinoma, $n = 512$; squamous carcinoma, $n = 475$), expression of miR-21-5p was significantly elevated, whereas that of DGKB was suppressed. (D) Comparative real-time quantitative polymerase chain reaction (qPCR) analysis revealed that clinical samples of brain-metastatic lung cancer had significantly higher miR-21-5p expression levels and lower DGKB expression levels than did primary lung cancer samples ($n = 10$ each group). (E) qRT-PCR analysis of expression of DGKB and miR-21-5p expression in MacKay Memorial Hospital -NSCLC cohort ($n = 10$) compared to normal. ***$P < 0.001$.

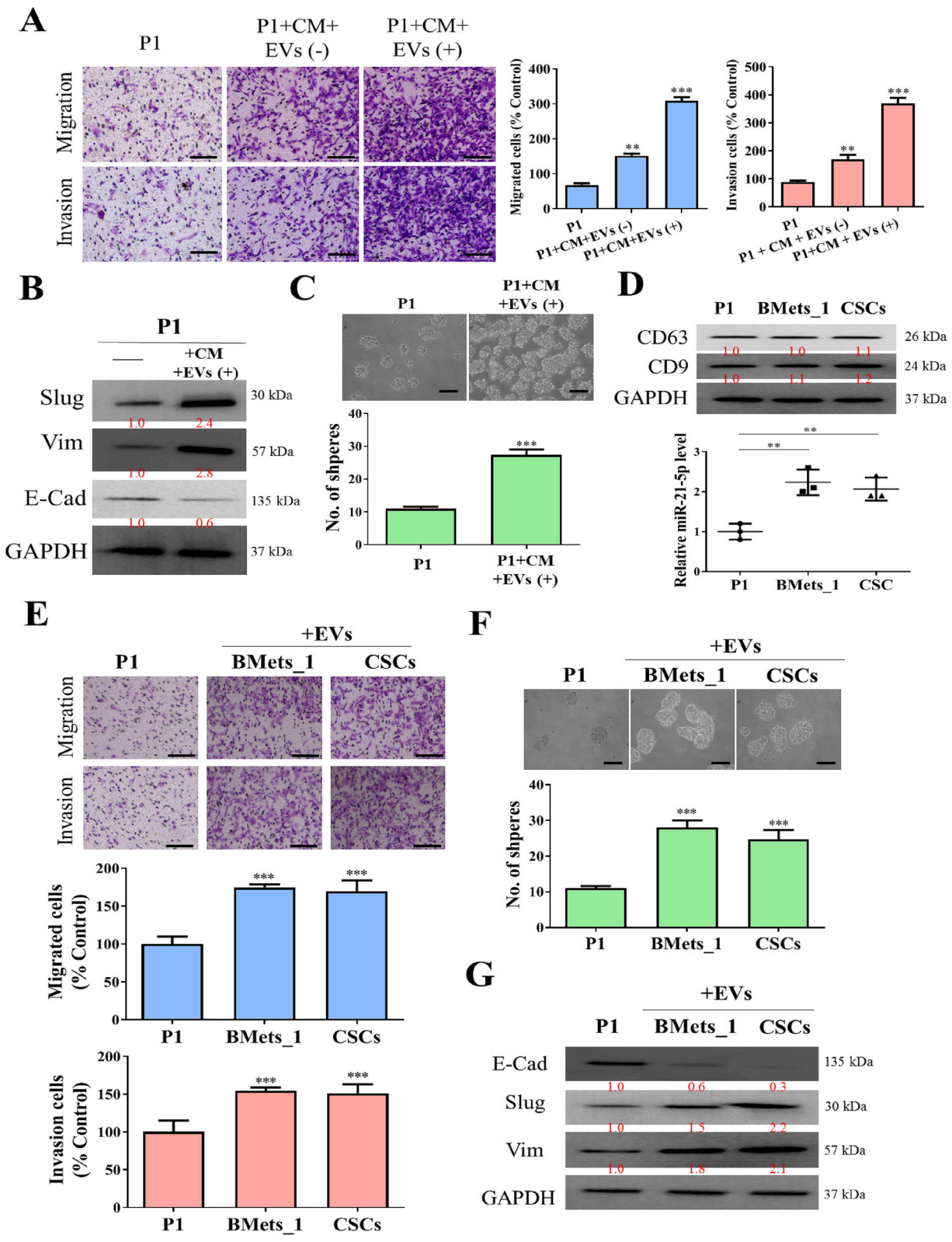

Fig. 2. Extracellular vesicles (EVs) enriched with miR-21 from brain-metastatic lung cancer cells (Bmets_1 cells) promoted tumorigenesis in nonmetastatic P1 primary lung cancer cells. (A) Conditional medium (CM), with EVs(+) or without EVs(−) from Bmets_1 cells promoted both migration (upper panels) and invasion (lower panels) in P1 primary cells compared to P1 control without exposure to CM or EVs. (B) P1 cells cultured with CM + EVs(+) exhibited increased expression of Slug and vimentin (Vim) and decreased expression of E-cadherin (E-cad). (C) P1 cells cultured with Bmets_1 CM + EVs(+) generated a significantly higher number of tumor spheres. (D) Western blot showing the expression of EV's associated marker (CD63 and CD9) of the EVs isolated from Bmests_1 cells and stem cell-like cells (CSCs), which demonstrated a higher miR-21-5p expression level than did those isolated from P1 cells. (E) P1 cells cultured with +EVs from Bmets_1 cells and CSCs exhibited significantly higher migratory (upper panels) and invasive (lower panels) abilities. (F) + EVs from Bmets_1 cells and CSCs enhanced the self-renewal ability of P1 cells. (G) Western blots revealed that P1 cells treated with +EVs from Bmets_1 cells and CSCs had significantly lower E-cadherin expression and higher Slug and vimentin expression. **P < 0.05; ***P < 0.001.

3.3. miR-21-containg EVs from BMets_1 cells promoted M2 polarization of macrophages

Tumor-associated macrophages (TAMs) are key stromal components within the TME and have been demonstrated to promote distant metastasis [24]. Here, we explored the functional relationship between EVs from BMets_1 cells and TAMs. When THP-1 cells were cultured with EVs from BMets_1, THP-1 exhibited an increased propensity toward M2 polarization. We noted that the secretion of M2-specific markers CD206 and CD163 was significantly increased, whereas that of M1 markers INF-γ and TNF-α was decreased (left panel, Fig. 3A); the secretion of M2 cytokines IL-6 and TGF-β was also increased, whereas that of M1 specific cytokines expressions such as INF-γ and TNF-α was decreased (right panel, Fig. 3A). We subsequently inhibited or overexpressed the production of miR-21-5p within BMets_1 cells by using miR-21 inhibitor/mimic and observed that the EVs from miR-21-5p silenced BMets_1 cells had a significantly lower level of miR-21-5p than did their control counterparts (left panel, Fig. 3B), suggesting that miR-21-5p was packaged into EVs within BMets_1 cells. Notably, EVs from miR-21-5p-silenced BMets_1 cells exhibited a significantly lower ability to promote M2 polarization; restoring the miR-21-5p level by using mimic molecules restored M2 polarization (right panel, Fig. 3B) as compared to the respective control. A similar phenomenon was observed in EVs derived from P1 cells with miR-21-5p expression silenced or upregulated (Fig. 3C). EVs derived from miR-21-5p-silenced BMets_1 cells exhibited a significantly lower ability to promote migration and invasion in P1 cells; upregulating miR-21-5p expression using mimic molecules restored this ability compared to the controls (Fig. 3D). EVs from miR-21-5p-silenced BMets_1 cell was significantly less capable of enhancing self-renewal ability in P1 cells compared to the controls; this ability was rescued by restoring the expression level of miR-21-5p (Fig. 3E).

3.4. Erk inhibitor ulixertinib suppressed lung tumorigenesis through downregulation of miR-21/Erk/STAT3 and upregulation of DGKB

Interestingly, an elevated level of miR-21 in lung cancer cells reportedly contributes to amplifying Erk/STAT3 signaling and gefitinib resistance [25]. In the present study, we also observed a significantly elevated miR-21 expression level which was negatively correlated with the expression of DGKB (Fig. 1). Here, we examined the potential usage of an Erk inhibitor ulixertinib for inhibiting lung tumorigenesis. We first observed that ulixertinib treatment significantly suppressed the viability of cancer cells. Notably, BMets_1 and H1623 cells (both with high metastatic potential) exhibited significantly lower DGKB expression levels, whereas expression levels were increased in the phosphorylated form of Erk and STAT3 (western blot below, Fig. 4A). In the non-metastatic lung cancer cells P1 and H2085, we observed the opposite expression profiles for DGKB and Erk/STAT3 (western blot below, Fig. 4A). Subsequently, we used the H1623 and H2085 cell lines as representative metastatic and nonmetastatic cells, respectively. Ulixertinib treatment prominently inhibited both migratory (Fig. 4B) and invasive (Fig. 4C) abilities in both the H1623 and H2085 cells. The self-renewal ability of lung cancer cells was significantly reduced by the ulixertinib treatment (Fig. 4D). Treatment with ulixertinib was associated with markedly reduced expression levels of Erk1/2, STAT3, survivin, and miR-21-5p, whereas the expression levels of DGKB and PARP increased (Fig. 4E). Correlation analysis of expression of above-mentioned markers in TCGA-LUAD 2016 samples as shown in Fig. 4F, also demonstrated the same trend, that is DGKB has an inverse correlation with the expression of PARP1, ERK1/2 (MAPK3), STAT3 and Survivn (BRIC5). Notably, the ulixertinib-treated H1623 and H2085 cells exhibited a significant reduction in the secretion of EVs (reduction in EV's marker, CD63 and CD9, western blot image above, Fig. 4G) and the expression level of miR-21-5p in EVs (Fig. 4G).

3.5. Ulixertinib treatment suppressed lung tumorigenesis and brain metastasis in vivo through the alteration of miR-21-5p/Erk signaling and upregulation of DGKB

Finally, we evaluated the potential lung cancer inhibitory effects of ulixertinib by using a PDX model, which involved inoculating BMets_1 cells orthotopically into the lungs of NOD/SCID mice. Ulixertinib-treated mice exhibited a significantly lower tumor burden than did the vehicle control (Fig. 5A). The incidence of brain metastasis was significantly reduced in the mice receiving ulixertinib; notably, mice bearing miR-21-5p-silenced (inhibitor) BMets_1 cell exhibited a similar phenotype to the ulixertinib-treated mice; in both of these groups, tumor burden and brain metastasis incidence were significantly lower than in the vehicle group (Fig. 5B) and no treatment associated toxicity was observed in the animal (below the panel, Fig. 5B). Further, the effect of treatment in the reduction of brain metastasis was also observed as compared to the respective control demonstrated in Fig. 5C. Most importantly, the most significant tumor inhibitory effects were observed in the mice bearing miR-21-5p-silenced BMets_1 cells treated with ulixertinib (the combined group; Fig. 5A and B). Furthermore, the expression of miR-21-5p was also assayed in the treated and controlled samples, showing a significant reduction in the expression of miR-21-5p (qRT-PCR analysis, Fig. 5D) Our immunohistochemical analysis indicated significantly reduced staining of PCNA (a marker for proliferation) and Erk, with increased DGKB and GFAP staining in the lung tumor sections (Fig. 5E). Sections from the miR-21-5p si group revealed similar staining patterns, and in the combined group, the lowest staining intensity was observed for PCNA and Erk, with the highest being observed for DGKB and GFAP (Fig. 5E). Real-time q-PCR experiments indicated that the tumor samples collected from the combined treatment group had lower miR-21-5p and higher DGKB expression levels than did those in the control group (right up panel, Fig. 5E), furthermore, reduction in Erk expression was seen (right down the panel, Fig. 5E). Relative to the vehicle group, the ulixertinib and miR-21-5p si groups also exhibited significantly lower miR-21-5p expression levels and higher DGKB expression levels.

4. Discussion

Metastatic lung cancer, both adenocarcinoma and squamous carcinoma subtypes, presents a serious challenge in patient treatment. Despite the development of novel therapeutics, the prognosis for patients with metastatic lung cancer remains extremely poor. Inhibiting the tumor growth alone is not sufficient because cancer cells often develop drug resistance. In novel drug development, the involvement of the TME has become as central a concern as the tumor cells [26]. TAMs are key players within the TME, and they have been demonstrated to directly participate in the development of drug resistance and distant metastasis through the secretion of protumor signaling molecules [27].

In this study, through an extensive literature review, we identified elevated levels of oncomiR miR-21 in lung adenocarcinoma and squamous carcinoma, with an inverse predictive correlation to its target gene, diacylglycerol kinase beta (DGKB). We observed that clinical BMets_1 cell promotes the M2 polarization of macrophages through miR-21-enriched EVs. According to one study, Mir-21 is an oncomiR that targets and suppresses the expression of tumor suppressors including PDCD4 and PTEN while increasing the expression of oncogenes such as EGFR and TGF-β [28]. Similarly, another study revealed that miR-21 is one of the most abundant microRNA species identified in the serum and EVs of patients with lung cancer and that it is correlated with poor prognosis [29].

In experiments with different cohorts of patients with lung cancer, we observed a strong inverse correlation between the expression levels of miR-21-5p and DGKB. We also noted that in this cohort, the expression of DGKB was significantly reduced (Fig. 1). This might be a signaling clue for brain metastasis. Our results indicate that the

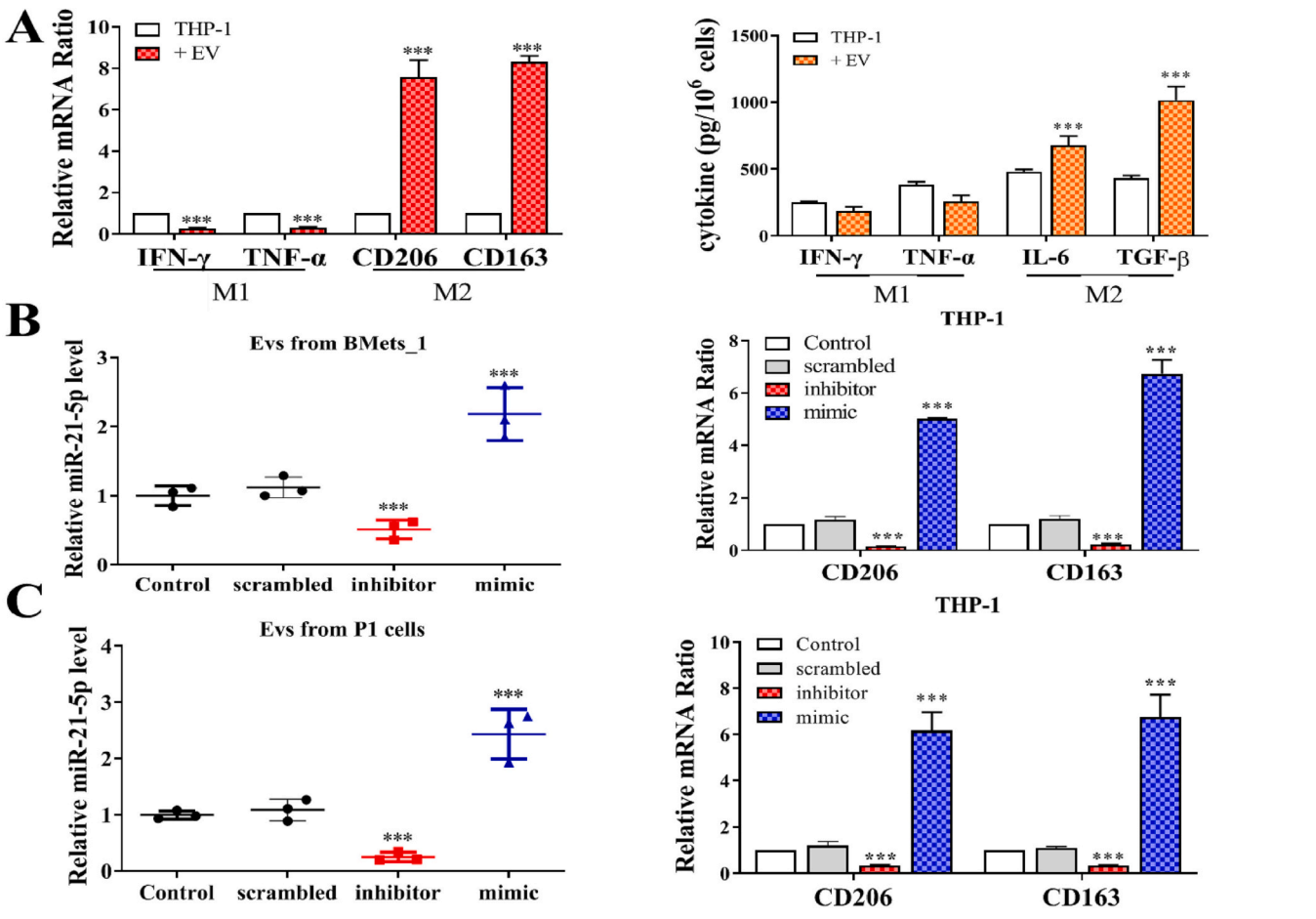

(caption on next page)

Fig. 3. EVs from Bmets_1 cells promoted M2 tumor-associated macrophage (TAM) polarization through the upregulation of miR-21-5p. (A) Real-time qPCR analysis of THP-1 cells cultured with EVs from BMets_1 cells indicated increased expression of M2 markers CD206 and CD163 but decreased expression of M1 markers INF-γ and TNF-α. ELISA assays revealed that THP-1 cells treated with BMets_1 EVs had significantly higher expression levels of M2 cytokines IL-6 and TGF-β and lower expression levels of M1 cytokines INF-γ and TNF-α. (B) Real-time qPCR analysis revealed a significantly reduced miR-21-5p expression level in EVs collected from the Bmets_1 cells treated with miR-21-5p inhibitor, mimic or scrambled control, whereas the opposite was true when miR-21-5p mimic molecules were transfected (left panel). EVs from Bmets_1 (treated with miR-21-5p inhibitor) exhibited a significantly lower ability to promote M2 markers (green bars), whereas the opposite was observed in EVs from Bmets_1 (treated with miR-21-5p mimic molecules; red bars; right panel). (C) Similar observations were made for EVs isolated from P1 cells transfected with miR-21-5p mimic molecules and THP-1 cultured with EVs from P1 (P1 cells treated with miR-21-5p mimic molecules); they exhibited significantly increased expression of M2 markers CD206 and CD163 (red bars). (D, E) EVs from Bmets_1 (miR-21-5p silenced) did not significantly increase the migratory and invasive abilities (D) or self-renewal potential (E) of P1 cells; these phenomena were reversed by restoring the expression of miR-21-5p as compared to respective control (scrambled, and non-treated control). ***$P < 0.001$.

suppression of miR-21-5p expression in brain-metastatic cells led to a reduction in metastatic potential, as indicated by the suppressed expression of slug and vimentin and increased expression of DGKB. These observations are supported by findings in a related study, where elevated miR-21-5p expression levels in lung cancer cells resulted in the promotion of tumorigenesis, including invasive ability and radioresistance [30]. Another study reported that EVs released by hypoxic NSCLC cells had elevated miR-21 expression levels and contributed to cisplatin resistance [31]. Our findings revealed that the silencing of miR-21-5p in BMets_1 cells resulted in reduced miR-21-5p expression in the EVs; the EVs with reduced levels of miR-21-5p were significantly less capable of promoting metastatic potential in nonmetastatic P1 cells as well as the M2 polarization of TAMs; these findings reveal another avenue through which miR-21-5p can extend its oncogenic effects—by suppressing tumor suppressors within the TME through EVs (Fig. 2). We also observed that EVs isolated from BMets_1 tumor spheres had elevated miR-21-5p expression levels, suggesting that lung cancer stem cells can also influence cancer stem cell niche through oncogenic EVs (Fig. 3). In this current study, EVs derived from tumor spheres (or CSCs) induced EMT in the nonmetastatic P1 cells by increasing the expression of slug and vimentin. Notably, a study revealed that miR-21 supports several metastasis-promoting signaling pathways, including HIF-1α, SMAD7, and PI3K/Akt/mTOR [32–34]. Another study revealed that the activation of STAT3 signaling can promote M2 polarization of TAMs [35,36] and that increased STAT3 activity was correlated with an increased miR-21 expression level; both observations help explain how miR-21-enriched EVs isolated from BMets_1 cells contribute to the M2 polarization of TAMs.

Based on our findings and results from previous studies, we examined the potential therapeutic functions of ulixertinib (an Erk inhibitor) for treating metastatic lung cancer by targeting both cancer cells and the TME. We observed that ulixertinib treatment markedly inhibited the tumorigenic properties of all lung cancer cell lines used in this study. Ulixertinib treatment not only reduced the expression levels of phosphorylated forms of Erk and STAT3 but also of miR-21-5p while increasing the DGKB expression level (Fig. 4). Diacylglycerol kinases (DGKs) are regulators of the intracellular concentration of diacylglycerol, a key second messenger, and have been reported to play key roles in carcinogenesis. The most studied member of the DGK family is DGKα. Studies have revealed that an increased DGKα expression level is correlated with metastatic potential in cancer cells [37–39] as well as that an increased DGKα expression level can facilitate cancer cell progression, including survival and distant metastasis [40,41].

Therefore, increased DGKα activity could potentially lead to the activation of the Erk signaling pathway, thereby promoting tumorigenesis. However, the role of DGKB in lung cancer remains unexplored. To the best of our knowledge, this is the first report to highlight DGKB's role as a tumor suppressor in NSCLC [42–44]. Our bioinformatics investigation demonstrated that DGKB expression was substantially suppressed in patients with lung cancer (both adenocarcinoma and squamous carcinoma subtypes) and was strongly correlated with high miR-21 expression. In addition, analysis from The Cancer Genome Atlas databases revealed that DGKB expression was consistently suppressed in multiple cancer types including bladder, breast, colon, liver, ovarian, prostate, pancreas, and brain (data not presented). DGKB was predicted to be one of the targets of miR-21; we observed that ulixertinib treatment significantly increased the expression of DGKB while reducing that of p-ERK and p-STAT3 and miR-21-5p (Fig. 4). In summary, our study underscores the tumor suppressor role of DGKB in NSCLC. We corroborated our theory using a patient-derived xenograft (PDX) mouse model (Fig. 5), where we noted a significant decrease in brain metastasis with either pharmacological inhibition through ulixertinib treatment or miR-21 expression silencing, as compared to the control group. The tumor inhibitory effect was recorded when both treatments were combined. *In vivo*, ulixertinib significantly reduced ERK expression and elevated DGKB levels, with a reduction in ERK expression aligning with suppressed miR-21-5p expression. Hence, understanding the role of EV-encapsulated miR-21-5p in the DGKB/ERK/STAT3 axis in lung cancer can shed light on lung cancer progression mechanisms and potential therapeutic targets.

5. Conclusion

We observed that EVs from malignant NSCLC cells were enriched with the oncomiR miR-21 and induced metastatic potential in nonmetastatic primary NSCLC cells (Fig. 6). In addition, miR-21-enriched EVs promoted the M2 polarization of TAMs. We demonstrated that the molecular link between DGKB and miR-21/Erk and ulixertinib treatment suppressed NSCLC tumorigenesis and brain metastasis by modulating this signaling pathway. Further investigation is warranted to support the usage of ulixertinib for treating brain-metastatic lung cancer in clinical settings.

Abbreviations

CSCs	cancer stem-like cells
TME	tumor microenvironment
EVs	extracellular vesicles
M2 TAMs	M2 polarization of macrophages
PDX	patient-derived xenograft
NSCLC	non-small-cell lung cancer
BMets_1 cells	brain-metastatic lung cancer cells
IRB	institutional review board
DGKs	diacylglycerol kinases

Ethics approval and consent to participate

Clinical samples were collected at MacKay Memorial Hospital (Taipei, Taiwan). All enrolled patients provided written informed consent for their tissues to be used for scientific research. The study was approved by the Institutional Review Board (IRB) of MacKay Memorial Hospital (IRB 20MMHIS500e), was conducted following the recommendations of the Declaration of Helsinki for biomedical research (MacKay Memorial Hospital Taipei, Taiwan), and followed the standard institutional protocol for human research. The animal study protocol was approved by the Animal Care and User Committee at MacKay Memorial Hospital (Affidavit of Approval of Animal Use Protocol # MacKay Memorial Hospital-MMH-A-S-111-10).

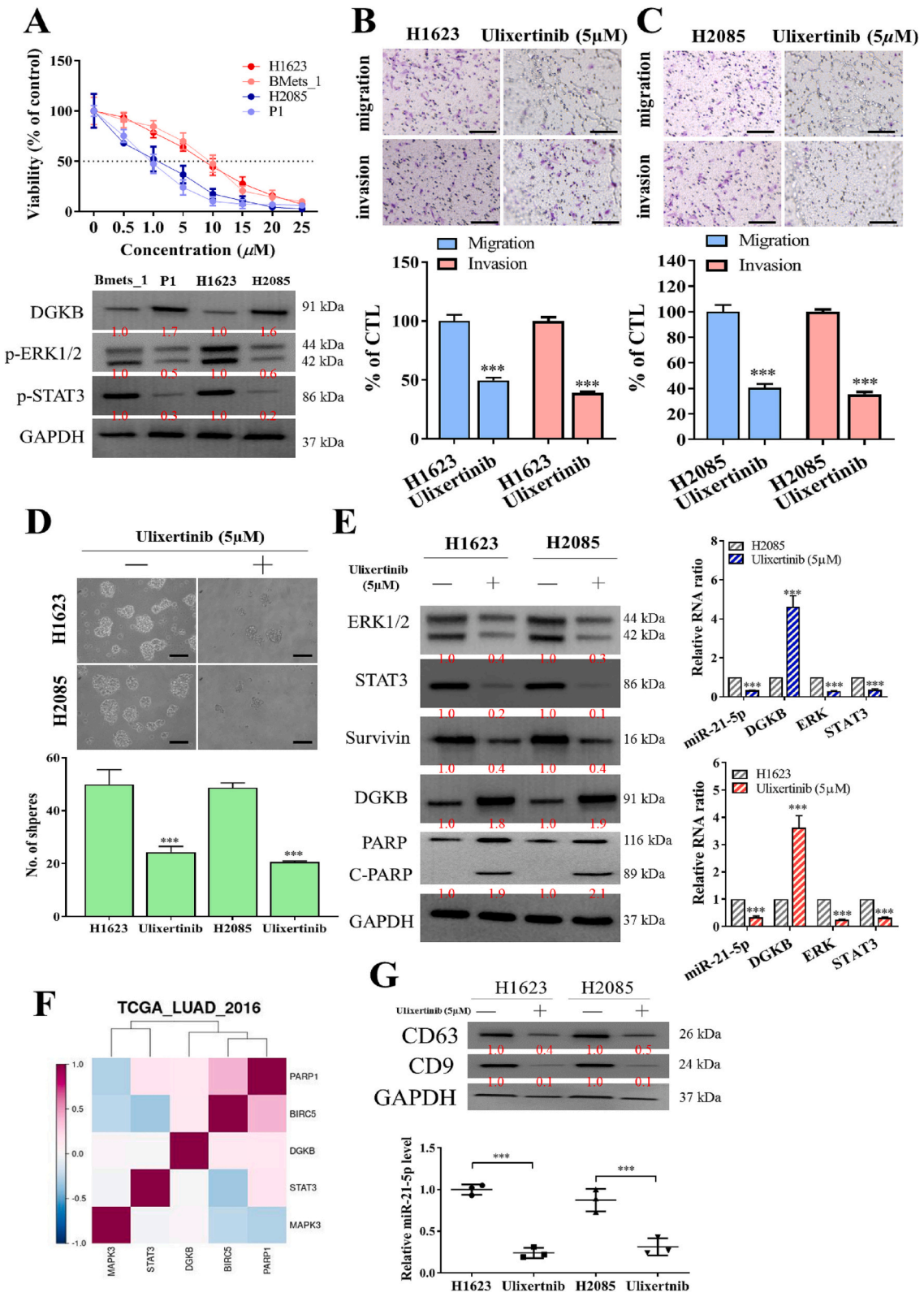

Fig. 4. Ulixertinib suppressed lung tumorigenesis and stemness *in vitro*. (A) Cell viability assay revealed that ulixertinib suppressed cell viability in BMets_1 and H1623 cells (metastatic lung cancer cells) and P1 and H2085 cells (nonmetastatic lung cancer cells). Western blots demonstrated expression differences among metastatic and nonmetastatic lung cancer cell lines (right panel). Metastatic cell lines (BMets_1 and H1623) exhibited markedly higher p-Erk and p-STAT3 expression levels but lower expression of DGKB than did their nonmetastatic counterparts (P1 and H2085). Ulixertinib treatment (5 μM, 24 h) significantly reduced the migratory (B) and invasive (C) abilities of H1623 and H2085 cells. (D) Ulixertinib (5 μM, 24 h) significantly inhibited the tumor formation ability in both H1623 and H2085 cells. (E) Ulixertinib treatment significantly reduced the expression of miR-21-5p, survivin, ERK, and STAT3 but increased that of DGKB and cleaved PARP in both cell lines. (F) correlation analysis of expression of DGKB, with PARP1, Erk1, STAT3 and Survivn using TCGA-LAUD samples. (G) Ulixertinib treatment reduced the miR-21-5p expression level in the EVs isolated from both H1623 and H2085 NSCLC cell lines. ***P < 0.001.

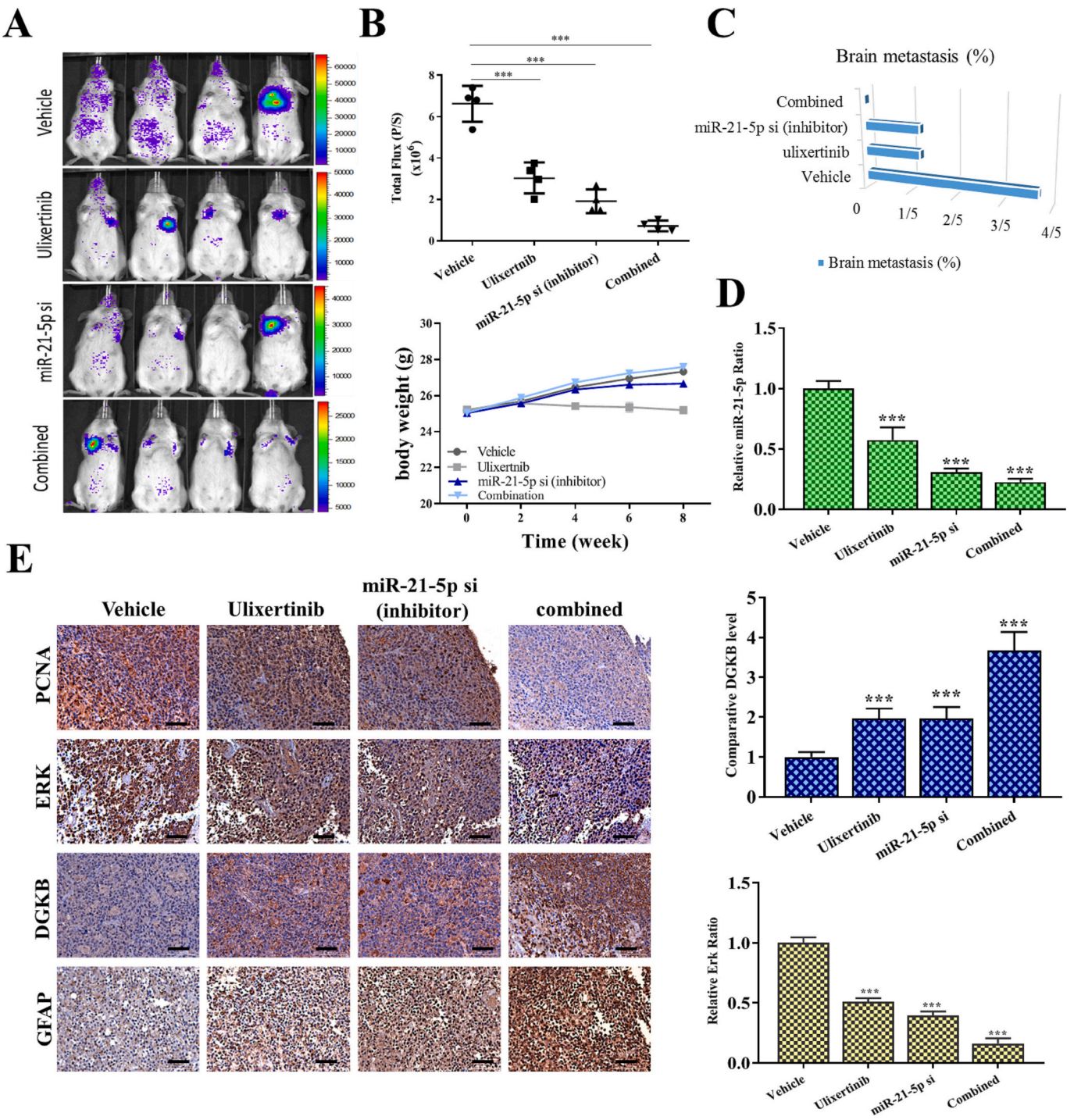

Fig. 5. Ulixertinib treatment suppressed lung tumorigenesis and brain metastasis *in vivo.* (A) Representative bioluminescence images of BMets_1 cells in a PDX mouse model 8 weeks after the orthotopic intrathoracic tumor injection and treatment. The tumor burden (represented by total photon flux) was lowest in the combined group (miR-21-5p-silenced BMets_1 cells with ulixertinib treatment), followed by ulixertinib treatment alone—miR-21-5p silenced BMets_1—(approximately equal intensity); the vehicle group exhibited the highest bioluminescence intensity. (B) Tumor burden and body weight of animals in the respective treatment. (C) plot demonstrate the percentage of brain metastasis. (D) qRT-PCR analysis of expression of miR_21-5p. (E) Immunohistochemical analysis of lung sections collected from all groups. The combined treatment group exhibited the lowest staining intensity for PCNA and ERK but the highest for DGKB and GFAP, followed by the ulixertinib treatment group and the miR-21-5p silenced group and vehicle group. Real-time qPCR analysis of tumor samples. The vehicle group had the highest miR-21-5p expression and the lowest DGKB expression of all the groups. The combined treatment group exhibited the lowest miR-21-5p expression but the highest DGKB expression. Erk 1/2 mRNA level was also significantly reduced in the samples from the combined treatment. ***$P < 0.001$.

Consent for publication

Not applicable.

Funding

This current study was backed by the National Science Council of Taiwan: Wen-Chien Huang (MOST111-2314-B195-020-MY3). This

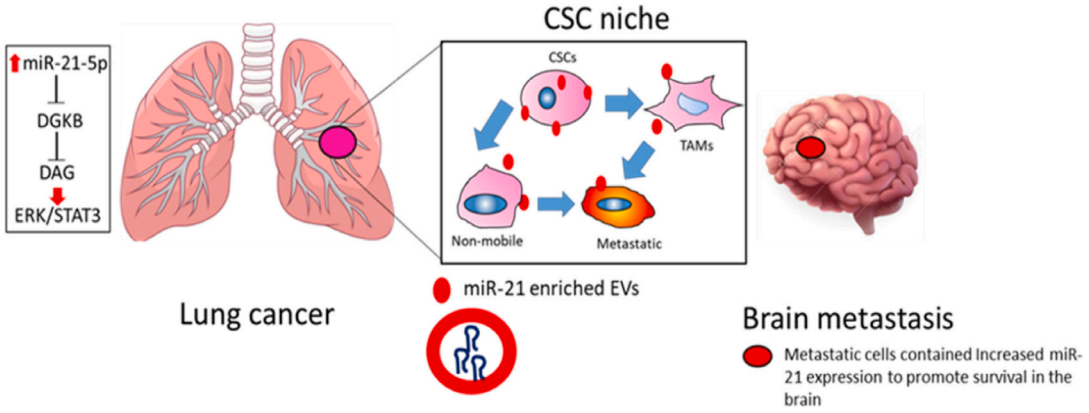

Fig. 6. Graphical summary of the lung cancer stem-like cell (CSCs) niche. CSCs secrete miR-21-enriched extracellular vesicles (EVs), which then transform both nonmobile cancer cells and macrophages into metastatic cells and M2 TAMs. Increased miR-21 expression activates the ERK/STAT3 signaling pathway and inhibits DGKB expression. Brain-metastatic lung cancer cells consistently express miR-21/ERK/STAT3 for survival. In the tumor microenvironment, cancer stem-like cells (CSCs) secrete miR-21-enriched extracellular vesicles (EVs). EVs transform both nonmobile cancer cells and macrophages into metastatic cells and M2 tumor-associated macrophages (TAMs). Increased miR-21 expression activates ERK/STAT3 signaling pathways by inhibiting DGKB expression. Brain-metastatic lung cancer cells consistently express miR-21/ERK/STAT3 for survival.

research was backed by a grant from the MacKay Memorial Hospital Joint Research Program (MacKay Memorial Hospital Joint Research Program) offered to Wen-Chien Huang (PC11107-5490).

CRediT authorship contribution statement

Conceived and designed the study: Tung-Yu Tiong & Chun-Hua Wang. Performed the experiments: Mei-lin Chan & Iat-Hang Fong. Analyzed the data: Vijesh Kumar Yadav. Bioinformatics: Narpati Wesa Pikatan. Wrote the manuscript: Tung-Yu Tiong and Wen-Chien Huang. Provided reagents, materials, experimental infrastructure and administrative oversight: Chi-Tai Yeh & Kuang-Tai Kuo. All authors read and approved the final version of the manuscript.

Declaration of competing interest

All authors are working for either university or hospitals. We claim that we do not have any actual or potential conflict of interest including any financial, personal or other relationships with other people or organizations within three years of beginning the work submitted that could inappropriately influence our work.

Data availability

The data sets used and analyzed in the current study are available from the corresponding author in response to reasonable requests.

Acknowledgments

We thank our laboratory assistant Mrs. Jenny Wang (From MacKay Memorial Hospital Taipei, Taiwan) for her technical assistance.

Appendix A. Supplementary data

Supplementary data to this article can be found online at https://doi.org/10.1016/j.lfs.2023.121945.

References

[1] H. Sung, J. Ferlay, R.L. Siegel, M. Laversanne, I. Soerjomataram, A. Jemal, et al., Global Cancer Statistics 2020: GLOBOCAN Estimates of Incidence and Mortality Worldwide for 36 Cancers in 185 Countries vol. 71, 2021, pp. 209–249.
[2] F. Petrella, S. Rizzo, I. Attili, A. Passaro, T. Zilli, F. Martucci, et al., Stage III non-small-cell lung cancer: an overview of treatment options, Current Oncol. (Toronto, Ont) 30 (2023) 3160–3175.
[3] R. Siegel, D. Naishadham, A. Jemal, Cancer statistics, 2013, CA Cancer J. Clin. 63 (2013) 11–30.
[4] Y. Xiao, P. Liu, J. Wei, X. Zhang, J. Guo, Y. Lin, Recent Progress in Targeted Therapy for Non-small Cell Lung Cancer vol. 14, 2023.
[5] M.D. Taylor, A.S. Nagji, C.M. Bhamidipati, N. Theodosakis, B.D. Kozower, C.L. Lau, et al., Tumor recurrence after complete resection for non-small cell lung cancer, Ann. Thorac. Surg. 93 (2012) 1813–1820 (discussion 20-1).
[6] S.B. Goldberg, J.N. Contessa, S.B. Omay, V. Chiang, Lung cancer brain metastases, Cancer J. (Sudbury, Mass) 21 (2015) 398–403.
[7] M. Frydrychowicz, A. Kolecka-Bednarczyk, M. Madejczyk, S. Yasar, G. Dworacki, Exosomes - structure, biogenesis and biological role in non-small-cell lung cancer, Scand. J. Immunol. 81 (2015) 2–10.
[8] A. Hoshino, B. Costa-Silva, T.L. Shen, G. Rodrigues, A. Hashimoto, M. Tesic Mark, et al., Tumour exosome integrins determine organotropic metastasis, Nature 527 (2015) 329–335.
[9] Z.H. Xu, Z.W. Miao, Q.Z. Jiang, D.X. Gan, X.G. Wei, X.Z. Xue, et al., Brain microvascular endothelial cell exosome-mediated S100A16 up-regulation confers small-cell lung cancer cell survival in brain, FASEB J. 33 (2019) 1742–1757.
[10] M. Saviana, G. Romano, P. Le, M. Acunzo, P. Nana-Sinkam, Extracellular vesicles in lung cancer metastasis and their clinical applications, Cancers (2021) 13.
[11] J. Bai, Z. Shi, S. Wang, H. Pan, T. Zhang, MiR-21 and let-7 cooperation in the regulation of lung cancer, Front. Oncol. 12 (2022), 950043.
[12] J.A. Sim, J. Kim, D. Yang, Beyond lipid signaling: pleiotropic effects of diacylglycerol kinases in cellular signaling, Int. J. Mol. Sci. (2020) 21.
[13] S. Parakh, M. Ernst, A.R. Poh, Multicellular effects of STAT3 in non-small cell lung cancer: mechanistic insights and therapeutic opportunities, Cancers (2021) 13.
[14] R. Sugiura, R. Satoh, T. Takasaki, ERK: a double-edged sword in cancer. ERK-dependent apoptosis as a potential therapeutic strategy for cancer, Cells (2021) 10.
[15] H.F. Bahmad, K. Cheaito, R.M. Chalhoub, O. Hadadeh, A. Monzer, F. Ballout, et al., Sphere-Formation Assay: Three-dimensional in Vitro Culturing of Prostate Cancer Stem/Progenitor Sphere-Forming Cells vol. 8, 2018.
[16] H. Hasan, I.S. Sohal, Z. Soto-Vargas, A.M. Byappanahalli, S.E. Humphrey, H. Kubo, et al., Extracellular vesicles released by non-small cell lung cancer cells drive invasion and permeability in non-tumorigenic lung epithelial cells, Sci. Rep. 12 (2022) 972.
[17] J. Dong, Z. Zhang, T. Gu, S.-F. Xu, L.-X. Dong, X. Li, et al., The Role of microRNA-21 in Predicting Brain Metastases From Non-small Cell Lung Cancer vol. 10, 2017, p. 185.
[18] F. Siegl, M. Vecera, I. Roskova, M. Smrcka, R. Jancalek, T. Kazda, et al., The significance of MicroRNAs in the molecular pathology of brain metastases, Cancers (2022) 14.
[19] M. Singh, N. Garg, C. Venugopal, R. Hallett, T. Tokar, N. McFarlane, et al., STAT3 pathway regulates lung-derived brain metastasis initiating cell capacity through miR-21 activation, Oncotarget. 6 (2015) 27461–27477.
[20] Z. Zhu, Q. Li, M. Xu, Qi ZJMSMIMJoE, C. Research, Effect of Whole-brain and Intensity-modulated Radiotherapy on Serum Levels of miR-21 and Prognosis for Lung Cancer Metastatic to the Brain vol. 26, 2020, pp. e924640–e924641.
[21] J. Dong, Z. Zhang, T. Gu, S.F. Xu, L.X. Dong, X. Li, et al., The role of microRNA-21 in predicting brain metastases from non-small cell lung cancer, OncoTargets Ther. 10 (2017) 185–194.
[22] L. Zhou, T. Lv, Q. Zhang, Q. Zhu, P. Zhan, S. Zhu, et al., The biology, function and clinical implications of exosomes in lung cancer, Cancer Lett. 407 (2017) 84–92.
[23] C. Bica-Pop, R. Cojocneanu-Petric, L. Magdo, L. Raduly, D. Gulei, I. Berindan-Neagoe, Overview upon miR-21 in lung cancer: focus on NSCLC, Cell. Mol. Life Sci. 75 (2018) 3539–3551.

[24] C. Dong, X. Liu, H. Wang, J. Li, L. Dai, J. Li, et al., Hypoxic non-small-cell lung cancer cell-derived exosomal miR-21 promotes resistance of normoxic cell to cisplatin, OncoTargets Ther. 12 (2019) 1947–1956.
[25] Z. Xu, X. Liu, H. Wang, J. Li, L. Dai, J. Li, et al., Lung adenocarcinoma cell-derived exosomal miR-21 facilitates osteoclastogenesis, Gene 666 (2018) 116–122.
[26] Z. Guo, J. Song, J. Hao, H. Zhao, X. Du, E. Li, et al., M2 macrophages promote NSCLC metastasis by upregulating CRYAB, Cell Death Dis. 10 (2019) 377.
[27] N.N. Parayath, A. Parikh, M.M. Amiji, Repolarization of tumor-associated macrophages in a genetically engineered nonsmall cell lung cancer model by intraperitoneal administration of hyaluronic acid-based nanoparticles encapsulating microRNA-125b, Nano Lett. 18 (2018) 3571–3579.
[28] F. Xu, W.Q. Cui, Y. Wei, J. Cui, J. Qiu, L.L. Hu, et al., Astragaloside IV inhibits lung cancer progression and metastasis by modulating macrophage polarization through AMPK signaling, J. Exp. Clin. Cancer Res. 37 (2018) 207.
[29] Z. Yao, J. Zhang, B. Zhang, G. Liang, X. Chen, F. Yao, et al., Imatinib prevents lung cancer metastasis by inhibiting M2-like polarization of macrophages, Pharmacol. Res. 133 (2018) 121–131.
[30] K. Wu, Q. Chang, Y. Lu, P. Qiu, B. Chen, C. Thakur, et al., Gefitinib resistance resulted from STAT3-mediated Akt activation in lung cancer cells, Oncotarget 4 (2013) 2430–2438.
[31] X. Xue, Y. Liu, Y. Wang, M. Meng, K. Wang, X. Zang, et al., MiR-21 and MiR-155 promote non-small cell lung cancer progression by downregulating SOCS1, SOCS6, and PTEN, Oncotarget 7 (2016) 84508–84519.
[32] F. Klemm, J.A. Joyce, Microenvironmental regulation of therapeutic response in cancer, Trends Cell Biol. 25 (2015) 198–213.
[33] N.E. Sounni, A. Noel, Targeting the tumor microenvironment for cancer therapy, Clin. Chem. 59 (2013) 85–93.
[34] S. Wahlin, B. Nodin, K. Leandersson, K. Boman, K. Jirström, Clinical impact of T cells, B cells and the PD-1/PD-L1 pathway in muscle invasive bladder cancer: a comparative study of transurethral resection and cystectomy specimens, Oncoimmunology. 8 (2019), e1644108.
[35] I. Datar, M.F. Sanmamed, J. Wang, B.S. Henick, J. Choi, T. Badri, et al., Expression analysis and significance of PD-1, LAG-3, and TIM-3 in human non-small cell lung cancer using spatially resolved and multiparametric single-cell analysis, Clin. Cancer Res. 25 (2019) 4663–4673.
[36] S. Xu, L. Shi, High expression of miR-155 and miR-21 in the recurrence or metastasis of non-small cell lung cancer, Oncol. Lett. 18 (2019) 758–763.
[37] H. Dejima, H. Iinuma, R. Kanaoka, N. Matsutani, M. Kawamura, Exosomal microRNA in plasma as a non-invasive biomarker for the recurrence of non-small cell lung cancer, Oncol. Lett. 13 (2017) 1256–1263.
[38] M. Feng, J. Zhao, L. Wang, J. Liu, Upregulated expression of serum exosomal microRNAs as diagnostic biomarkers of lung adenocarcinoma, Ann. Clin. Lab. Sci. 48 (2018) 712–718.
[39] Y. Yuan, X.Y. Xu, H.G. Zheng, B.J. Hua, Elevated miR-21 is associated with poor prognosis in non-small cell lung cancer: a systematic review and meta-analysis, Eur. Rev. Med. Pharmacol. Sci. 22 (2018) 4166–4180.
[40] X.L. Fu, W. Duan, C.Y. Su, F.Y. Mao, Y.P. Lv, Y.S. Teng, et al., Interleukin 6 induces M2 macrophage differentiation by STAT3 activation that correlates with gastric cancer progression, Cancer Immunol. Immunother. 66 (2017) 1597–1608.
[41] X. Hao, B. Sun, L. Hu, H. Lähdesmäki, V. Dunmire, Y. Feng, et al., Differential gene and protein expression in primary breast malignancies and their lymph node metastases as revealed by combined cDNA microarray and tissue microarray analysis, Cancer. 100 (2004) 1110–1122.
[42] G. Baldanzi, S. Cutrupi, F. Chianale, V. Gnocchi, E. Rainero, P. Porporato, et al., Diacylglycerol kinase-alpha phosphorylation by Src on Y335 is required for activation, membrane recruitment and Hgf-induced cell motility, Oncogene. 27 (2008) 942–956.
[43] A. Marchet, S. Mocellin, C. Belluco, A. Ambrosi, F. DeMarchi, E. Mammano, et al., Gene expression profile of primary gastric cancer: towards the prediction of lymph node status, Ann. Surg. Oncol. 14 (2007) 1058–1064.
[44] E. Rainero, P.T. Caswell, P.A. Muller, J. Grindlay, M.W. McCaffrey, Q. Zhang, et al., Diacylglycerol kinase α controls RCP-dependent integrin trafficking to promote invasive migration, J. Cell Biol. 196 (2012) 277–295.